mathematics

MDPI

Article

Adaptive Interval Type-2 Fuzzy Neural Network Sliding Mode Control of Nonlinear Systems Using Improved Extended State Observer

Lunhaojie Liu [1], Juntao Fei [1,2,*] and Xianghua Yang [2]

[1] College of IoT Engineerin, Jiangsu Key Lab. of Power Transmission and Distribution Equipment Technology, Hohai University, Changzhou 213022, China
[2] College of Mechanical and Electrical Engineering, Hohai University, Changzhou 213022, China
* Correspondence: jtfei@hhu.edu.cn

Abstract: An adaptive sliding mode control (ASMC) based on improved linear extended state observer (LESO) is proposed for nonlinear systems with unknown and uncertain dynamics. An improved LESO is designed to estimate total disturbance of the uncertain nonlinear system, and an interval type-2 fuzzy neural network (IT2FNN) is used to optimize and approximate the observe bandwidth of LESO, and the adaptive parameter tuning is realized based on the gradient descent (GD) method. Based on the total disturbance estimated by LESO, an ASMC strategy is designed to ensure the system stability. By adapting the sliding mode gain, the observation performance of LESO compared to the total disturbance can be better utilized, and system chattering is reduced. Finally, some simulation results are given which show that the proposed control strategy has a good control effect, strong practicability, and wide versatility.

Keywords: adaptive sliding mode control; linear extended state observer; interval type 2 fuzzy neural network; gradient descent

MSC: 68T07; 93C40; 93C42

Citation: Liu, L.; Fei, J.; Yang, X. Adaptive Interval Type-2 Fuzzy Neural Network Sliding Mode Control of Nonlinear Systems Using Improved Extended State Observer. *Mathematics* **2023**, *11*, 605. https://doi.org/10.3390/math11030605

Academic Editors: Fangzheng Gao and Zhongcai Zhang

Received: 4 January 2023
Revised: 18 January 2023
Accepted: 20 January 2023
Published: 25 January 2023

1. Introduction

In practical applications, most systems are nonlinear and have unknown disturbances, including matched and mismatched disturbances [1]. Due to the existence of unknown nonlinearities, it is not easy to design controllers for a class of systems with unknown uncertainties. For the past few decades, most applications have simply used traditional linear control methods to design controllers on inaccurate nominal models, which are increasingly shown to compromise accuracy and overall performance. In addition, control strategies that do not depend on models, such as PID [2], adaptive technology [3,4], fuzzy logic system [5,6], and neural network [7], have achieved certain results in the application of unknown model information, but their parameter adjustment has great blindness and uncertainty, and none of them have the versatility of control strategies, which means that the designed controllers and parameters cannot be simply extended from one application object to other application objects.

Recently, sliding mode control (SMC) has been widely used in nonlinear system control [8–11]. Due to its unique high-frequency switching characteristics, it is insensitive to disturbances. Therefore, in many applications, traditional SMC is used to offset the effects of lumped uncertainty. The traditional SMC needs to know the upper bound of the perturbation to select the appropriate switching term gain. However, in most scenarios, the form and size of the disturbance cannot be known in advance, so an excessively large switching term gain will be given to ensure the stability of the system, which will lead to severe output chattering. In response to this problem, many new forms of sliding mode

control strategies, such as terminal sliding mode control (TSMC) [12,13], super-twisting sliding mode control (STSMC) [14,15], and adaptive sliding mode control (ASMC) [16,17], have been widely studied and applied. Among them, the ASMC combines the adaptive technology, which can automatically adjust the sliding mode gain according to the real-time state of the system, thus solving the problem that the upper bound of the total disturbance is unknown. In [18], a robust ASMC is proposed for boost converter control where the load and input voltage are unknown. However, when there are too many unknown uncertainties in the system, such as unmodeled dynamics, parameter changes, external disturbances, etc., the simple sliding mode control strategy cannot realize the complete compensation of disturbances. Therefore, to improve the anti-disturbance ability and overall performance of the system, effective strategies must be taken to estimate and automatically compensate the unknown uncertainty, and then, the system can be effectively controlled by related strategies, such as SMC.

Therefore, how to estimate the total disturbance becomes the key to the control of uncertain nonlinear systems. As of recently, neural networks (NN) and model-based observers are two effective disturbance estimation techniques. The former realizes the identification and estimation of unknown disturbances through online learning and parameter adjustment [19–22], while the latter reconstructs the forms of states and disturbances from system errors and control inputs by constructing appropriate differential equations [23]. In [24], a recurrent neural network (RNN) controller, which was trained online using a dynamic back-propagation algorithm, was proposed to control an ultrasonic motor drive. In addition, a new RNN structure and a TSMC strategy with a new recurrent neural network were proposed in [25,26], improving control accuracy and robustness. In [27], a novel Hermite neural network-based second-order sliding-mode (HNN-SOSM) controller is proposed for the synchronous reluctance motor drive system. A self-constructing fuzzy neural network and self-evolving Chebyshev fuzzy neural network are proposed for active power filter in [28,29]. However, even though NN has strong learning and estimation abilities—and it can solve unknown and uncertain problems—its computational complexity is high, and the parameter learning strategy is ambiguous and difficult to design, which brings difficulties to its wide application.

Fortunately, on the other hand, after the observer was first proposed by Luenberger [30], there has been a growing body of work on the estimation of states and disturbances [31–33]. A high-gain extended state observer was used to estimate the system state and disturbance in [34], which is applied for electro-hydraulic systems. However, high-gain observers are sensitive to noise, and high-gain can easily cause the system to diverge and oscillate. Recently, a new method called active disturbance rejection control (ADRC) has been widely studied and used due to its inherent disturbance immunity and model-free property [23,35]. The complete ADRC includes three parts: tracking differentiator, fastest control rate, and extended state observer (ESO). ESO is the core active disturbance rejection module, which can be divided into nonlinear and linear, respectively called nonlinear ESO (NESO) and linear ESO (LESO). In [36], an ADRC-based controller was proposed for a magnetic rodless pneumatic cylinder, where a NESO was used to estimate the nonlinear dynamics, and the self-stabilizing region theory was used to prove the NESO's convergence. In [37], a convergence theory with explicit error estimates was provided, and the convergence of NESO, consisting of linear and fractional power functions, was demonstrated. Although NESO has achieved effective applications and extensive research, its complex structure and difficult parameter tuning are not conducive to engineering practice and expanded applications. Then, the structure and design of LESO was first proposed by Gao in [38]. Compared with NESO, the proposed LESO has the characteristics of simple structure and greatly simplifies the parameter tuning through the bandwidth parameterization method. Since then, LESO-based ADRC strategies have been widely used in practical industries such as air–fuel ratio control [39] and nonlinear servomechanisms [40], etc. In [41], the parameter tuning problem of LESO was studied, stating the widely used LADRC bandwidth tuning method is equivalent to tuning the two time constants of the setpoint filter and the robust

filter in the internal model control. However, both the bandwidth tuning method and the IMC-based tuning method only slightly simplify the parameter tuning process and reduce the tuning dimension, and they still require careful manual adjustments of parameters such as observation bandwidth or time constant. Furthermore, in [42], the relationship between the perturbed estimation error and the observation bandwidth is explicitly given. Therefore, aiming at the difficulty of parameter design, according to the perturbation relation and the bandwidth tuning method, an interval type-2 fuzzy neural network is designed to learn the observer bandwidth based on the gradient descent (GD) method.

Therefore, in this paper, a LESO is used to approach the total disturbance of a class of uncertain nonlinear systems to realize the active compensation of the disturbance. For the inevitable observation error, ASMC is used to ensure the stability of the uncertain system, fully cooperating with the observer to estimate the disturbance and avoid excessive control gain to weaken the chattering. Aiming at the problem of LESO parameter design, based on the parameter adjustment of the bandwidth method, the IT2FNN, based on the GD method, is proposed for the first time to estimate the observer bandwidth and minimize the estimation error. The proposed controller combines LESO, IT2FNN, and ASMC. Compared with existing state-of-the-art research, the main contributions of the proposed strategy include:

(1) The proposed control strategy is designed for a class of uncertain systems. It does not depend on an accurate mathematical model. It only needs to know the information of the model order to design an efficient controller. The simulation results show that the proposed controller has good versatility and practicability.
(2) Compared with existing work, the improved LESO does not need to manually select the observation coefficients, and it can automatically learn to estimate the observer bandwidth through the IT2FNN—based on the GD method—and then give the observation coefficients, according to the bandwidth method, to minimize the estimation error. Compared with NESO, although the improved LESO loses a certain estimation accuracy, it greatly simplifies the observer design and parameter adjustment process, which is more conducive to practical application and expansion.
(3) The IT2FNN, based on the GD method, was first proposed to estimate the observer bandwidth of LESO. Through the designed learning process, the neural network can adaptively learn the optimal parameter values to minimize the estimation error. Compared with reinforcement learning methods, the proposed strategy is more practical and has low computational complexity.
(4) The combination of ASMC and improved LESO technology enables a coordinated duality of the control process. LESO acts as a forerunner to actively compensate the unknown uncertainty of the system, and ASMC, as the main controller, increases the compensation for the residual disturbance relatively slowly. Such a binary coordinated control strategy can make the control process more visualized and clearer. The proposed controller can reduce the chattering of output while reducing the error and ensuring the optimal comprehensive performance.

This paper is organized as follows. In Section 2, a general model design for a class of uncertain nonlinear systems is introduced under the ADRC framework. In Section 3, a new ASMC with improved LESO is proposed. Simulation verifications are given in Section 4. Section 5 draws conclusions.

2. Problem Statement and Preliminaries

Consider a class of single-input single-output (SISO) N-order general uncertain nonlinear systems

$$\begin{cases} \dot{x}_1 = x_2 \\ \dot{x}_2 = x_3 \\ \cdots \\ \dot{x}_n = f(X) + b(X)u + d(t) \\ y = x_1 \end{cases} \tag{1}$$

where

$$X = \begin{bmatrix} x_1 & x_2 & \dots & x_n \end{bmatrix}^T,$$

X is a system state, $d(t)$ is an external disturbance, y is a system output, $f(X)$ and $b(X)$ are the nonlinear dynamics and control gains of the system, respectively, which satisfy the following two assumptions.

Assumption 1. *The nonlinear dynamic $f(X)$ is bounded in absolute value, expressed as*

$$|f(X)| < f_b(X) \tag{2}$$

where $f_b(X)$ is a positive bounded function.

Assumption 2. *The control gain $b(X)$ is a positive function greater than 0 and is lower bounded, expressed as*

$$b(X) > b_l(X) \tag{3}$$

where$b_l(X)$ is a positive bounded function.

Remark 1. *In practical applications, considering factors such as parameter changes, measurement errors, and modeling errors, the system dynamics and control gains cannot be accurately obtained. Simply using the nominal model to design the controller will bring large unknown uncertainties, and cannot achieve high-precision, strong adaptive control. Therefore, in this article, we will consider the worst-case scenario, where $f(X)$ is completely imprecise, and treat it as an entirely unmodeled dynamic. Fortunately, the modeling error of the control gain is often not large, which will not have a great impact on the control effect. Especially in the ADRC framework, the control gain can be manually selected as a nominal value, and its estimation error will be estimated by the extended state observer. In addition, under the framework of active disturbance rejection control, the concept of total disturbance $f_{td}(X)$ is proposed and defined as*

$$f_{td}(X) = f(X) + (b - b_o)u + d(t)$$

which includes the unknown dynamics of the system and external disturbances, where b_o is the actual control gain adopted by the controller. And the total disturbance $f_{td}(X)$ is expanded into a new state x_{n+1} , that is

$$x_{n+1} = f_{td}(X).$$

Therefore, the system can be rewritten as the following extended $n+1$-order differential equation:

$$\begin{cases} \dot{x}_1 = x_2 \\ \dot{x}_2 = x_3 \\ \dots \\ \dot{x}_n = x_{n+1} + b_o u \\ \dot{x}_{n+1} = h \\ y = x_1 \end{cases} \tag{4}$$

where x_{n+1} is the expanded state variable, and h is the derivative of the total disturbance, which can always be bounded.

3. Proposed Control System

The block diagram of the proposed control strategy for a class of uncertain nonlinear systems is given in Figure 1. As can be seen from the figure, the controller includes three components: IT2FNN, LESO, and ASMC. Among them, IT2FNN is designed to optimize the LESO parameters, thus self-learning to estimate the observer bandwidth to achieve parameter self-tuning. Then, LESO is used to estimate the total disturbance of the nonlinear system and, then, realize the feedforward compensation of uncertainty. ASMC can offset the estimation error of the disturbance. The control goal is to design an effective controller so that the system state X tracks the reference signal X_m asymptotically.

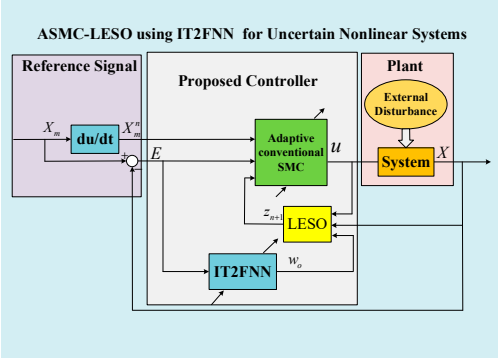

Figure 1. Block diagram of the proposed control systems.

3.1. Design of Linear Extended State Observer

LESO is obtained by simplifying the design of NESO. The construction of the nonlinear feedback function in NESO is very complicated, and the parameter tuning is also difficult. Therefore, although the performance of linear feedback in LESO will be slightly worse in theory, it is obviously worth sacrificing some estimated performance in exchange for the simplicity and practicality of the design. Therefore, this section will design LESO for the $(N+1)$-order uncertain nonlinear system after expansion, and the design process is given as follows.

$$\begin{cases} \dot{z}_1 = z_2 - \beta_1(z_1 - x_1) \\ \dot{z}_2 = z_3 - \beta_2(z_1 - x_1) \\ \cdots \\ \dot{z}_n = z_{n+1} - \beta_n(z_1 - x_1) + b_o u \\ \dot{z}_{n+1} = -\beta_{n+1}(z_1 - x_1) \end{cases} \tag{5}$$

where

$$\mathrm{Z} = [z_1 \quad z_2 \quad \ldots \quad z_{n+1}]^T, L = [\beta_1 \quad \beta_2 \quad \ldots \quad \beta_{n+1}]^T,$$

Z is the observed value of system states and extended total disturbance, while L is the observer gain.

Remark 2. *Because $f(X)$ is regarded as the unmodeled dynamic described in Remark 1, which is part of the total disturbance, $f(X)$ did not occur in the observer equation Equation (5). It is worth mentioning that if part of the accurate information of the system can be obtained, it can be directly added into the observer equation, which is conducive to further improving the estimation accuracy of the observer.*

The observation error is defined as

$$e_{o_i} = x_i - z_i \; i = 1, 2, \ldots, n+1.$$

The difference between the system equation and the observer equation can find the observation error equation as follows

$$\begin{cases} \dot{e}_{o_1} = e_{o_2} - \beta_1 e_{o_1} \\ \dot{e}_{o_2} = e_{o_3} - \beta_2 e_{o_1} \\ \cdots \\ \dot{e}_{o_n} = e_{o_{n+1}} - \beta_n e_{o_1} \\ \dot{e}_{o_{n+1}} = h - \beta_{n+1} e_{o_1} \end{cases} \tag{6}$$

The observation error equation can be rewritten in vector form as follows

$$\dot{E}_o = A_e E_o + Mh \tag{7}$$

where

$$A_e = \begin{bmatrix} -\beta_1 & 1 & 0 & 0 & 0 \\ -\beta_2 & 0 & 1 & 0 & 0 \\ \vdots & 0 & 0 & \ddots & 0 \\ -\beta_n & 0 & 0 & 0 & 1 \\ -\beta_{n+1} & 0 & 0 & 0 & 0 \end{bmatrix} \tag{8}$$

$$E_o = \begin{bmatrix} e_{o_1} & e_{o_2} & \cdots & e_{o_n} & e_{o_{n+1}} \end{bmatrix}^T \tag{9}$$

$$M = \begin{bmatrix} 0 & 0 & \cdots & 0 & 1 \end{bmatrix}^T \tag{10}$$

it can be seen that as long as the poles of the characteristic polynomial

$$\lambda(s) = s^{n+1} + \beta_1 s^n + \cdots + \beta_n s + \beta_{n+1}$$

of A_e are all in the left half-plane. Additionally, it can be assumed that h is bounded. Then, LESO is proven to be bounded-input bounded-output stable.

Therefore, the observation gain of the LESO can be obtained by the pole configuration method. Gao [32] proposed a bandwidth parameterization method to select the observation gain and configure the poles of the characteristic polynomial at $-w_o$, where w_o is the observation bandwidth. Therefore, the following equation can be solved to obtain the specific observation gain value:

$$\lambda(s) = s^{n+1} + \beta_1 s^n + \cdots + \beta_n s + \beta_{n+1} = (s + w_o)^{n+1} \tag{11}$$

3.2. Structure of Interval Type-2 Fuzzy Neural Network

Although the parameter setting of LESO can be completed by introducing the observation bandwidth, the selection of the observation bandwidth is still a mysterious problem, and a reasonable observation bandwidth value cannot be set in many application scenarios. When the observation bandwidth is selected larger, the observation speed is fast, but if it is too large, it will be too sensitive to noise and lead to divergence, and if it is too small, there will be serious phase lag. Therefore, it is imperative to use adaptive technology, especially the neural network optimization strategy with self-learning ability, to obtain the observation bandwidth of real-time uncertain nonlinear systems. Then, the following section will first introduce the structure and characteristics of the IT2FNN adopted in this paper, and the learning optimization strategy will be given in the next section.

As shown in Figure 2, The IT2FNN is a five-layer structure which is multiple input single output (MISO). The IT2FNN structure can be divided into the antecedent layer part and the consequent layer part. The computation and operation process of each layer in IT2FNN is given as follows. For a more detailed description, please refer to [37].

(1) Antecedent layer part: The antecedent layer contains the input layer and the membership layer. Additionally, the role of the antecedent layer is to obtain the input signal and use the type-2 fuzzy member function to perform nonlinear processing on the input signal to improve the distribution of the input signal, which is beneficial to the information extraction and optimal learning of the neural network. It is worth mentioning that, since there are few parameters in this layer, they are mainly the basis width and center vector in the type-2 fuzzy membership function, and they are easily obtained by a priori selection from the statistical features of the input signal. Therefore, instead of using the gradient optimization algorithm to calculate, it is better to directly use the expert experience to obtain the parameters of the leading layer. It not only simplifies the calculation amount of the neural network and optimizes the computing power but it also ensures that the antecedent layer of IT2FNN can abstract more effective and differentiated input information.

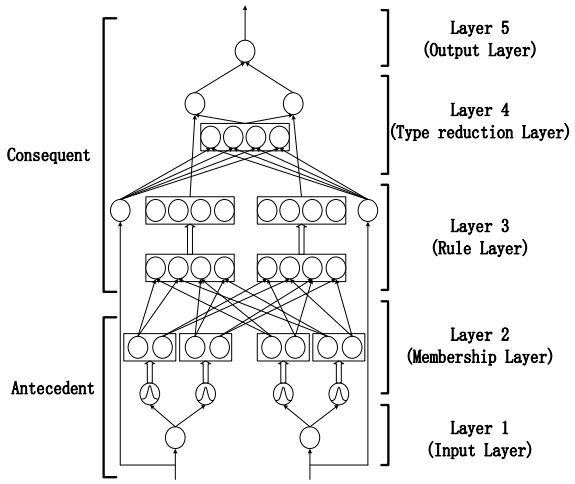

Figure 2. Network structure diagram of IT2FNN.

Layer 1: The input and output expressions of the input layer are as follows

$$y_i^1(N) = x_i^1(N)\ i = 1, \cdots, I \tag{12}$$

where $x_i^1(N)$ and $y_i^1(N)$ are the input and output of *i-th* node, respectively.

Layer 2: The input and output expressions of the membership layer are as follows

$$x_{i,j}^2(N) = y_i^1(N)\ j = 1, \cdots J \tag{13}$$

$$\overline{u}_{i,j}^2(N) = \exp\left(-\left(\frac{x_{i,j}^2 - c_{i,j}}{\overline{\sigma}_{i,j}}\right)^2\right) \tag{14}$$

$$\underline{u}_{i,j}^2(N) = \exp\left(-\left(\frac{x_{i,j}^2 - c_{i,j}}{\underline{\sigma}_{i,j}}\right)^2\right) \tag{15}$$

where $c_{i,j}$ is a center vector; $\overline{\sigma}_{i,j}$ and $\underline{\sigma}_{i,j}$ are the upper and lower base widths.

(2) Consequent layer part: The consequent layer part includes the rule layer, the type reduction layer, and the output layer, which is used to perform data derivation and calculation, based on the input information abstracted by the antecedent layer, and output the expected result.

Layer 3: The input and output expressions of the rule layer are as follows

$$\overline{w}_{i.j} = \overline{u}_{1,i} * \overline{u}_{1,j} \tag{16}$$

$$\underline{w}_{i.j} = \underline{u}_{1,i} * \underline{u}_{1,j} \tag{17}$$

$$\widetilde{\overline{w}}_{i,j} = \frac{\overline{w}_{i,j}}{\sum \overline{w}_{i,j}} \tag{18}$$

$$\widetilde{\underline{w}}_{i,j} = \frac{\underline{w}_{i,j}}{\sum \underline{w}_{i,j}} \tag{19}$$

where $\widetilde{\overline{w}}_{i,j}$ and $\widetilde{\underline{w}}_{i,j}$ are the upper bound and lower bound.

Layer 4: The input and output expressions of the type reduction layer are as follows

$$f_{i,j} = a_{i,j} * x_{i,j} + b_{i,j} \tag{20}$$

$$\overline{\phi} = \sum f_{i,j} * \widetilde{\overline{w}}_{i,j} \tag{21}$$

$$\underline{\phi} = \sum f_{i,j} * \underline{\widetilde{w}}_{i,j} \tag{22}$$

where $\overline{\phi}$ and $\underline{\phi}$ are the upper and lower output, respectively.

Layer 5: The input and output expressions of the output layer are as follows

$$y_o^5(N) = (1-q) * \overline{\phi} + q * \underline{\phi} \tag{23}$$

where q is a weighting factor; $y(N)$ is the final output of the IT2FNN.

The IT2FNN is used to approach the observation bandwidth w_o. The main idea is to use the system error and derivative of error as the inputs of the IT2FNN, adopt the optimization strategy based on GD method to adjust the network parameters, and estimate the observation bandwidth w_o. The detailed derivation of the parameter learning strategy of IT2FNN is presented in the next section.

3.3. Parameter Learning of IT2FNN

First, define the loss function E of IT2FNN to estimate bandwidth as

$$E = \frac{1}{2}(x_1 - z_1)^2 = \frac{1}{2}e_{o_1}^2 \tag{24}$$

Then, define δ^5 as the gradient of the loss function to the network output of the IT2FNN, which can be calculated as

$$\delta^5 = -\frac{\partial E}{\partial y_o^5} = -\frac{\partial E}{\partial e_{o_1}}\frac{\partial e_{o_1}}{\partial y_o^5} = -e_{o_1}\frac{\partial e_{o_1}}{\partial w_o} \tag{25}$$

From the literature [36], it can be known that the relationship between the observation error and the bandwidth is as follows

$$|e_{o_1}(t)| \leq \left| \frac{\sum_{i=1}^{n+1} |e_{o_i}(0)|}{w_o^{n+1}} \right| + \frac{\delta v}{w_o^{n+1}} + \frac{\delta \mu}{w_o^{2n+2}} \tag{26}$$

where v and μ are positive constants computable by order, and δ is also a positive constant, which satisfies $\delta \geq h$.

Therefore, the high-order small quantities can be ignored, and the relationship between the bandwidth and the estimation error can be obtained by simplifying the above formula as

$$|e_{o_1}(t)| \approx \frac{\tau}{w_o^{n+1}} \tag{27}$$

where τ is a large positive constant.

Then, the following can be deduced

$$\frac{\partial e_{o_1}}{\partial w_o} = -\frac{(n+1)\tau}{w_o^{n+2}} sign(e_{o_1}) \tag{28}$$

Substituting Equation (28) into δ^5 Equation (25) gets

$$\delta^5 = \frac{(n+1)\tau}{w_o^{n+2}} |e_{o_1}| \tag{29}$$

Then, the update rate of the weights can be calculated by back-propagation through the gradient method and the chain rule as follows.

The update law of the weight q is calculated as

$$\frac{\partial y_o^5}{\partial q} = \underline{\phi} - \overline{\phi} \tag{30}$$

$$\begin{aligned} \Delta q &= -\eta_q \frac{\partial E}{\partial q} = -\eta_q \frac{\partial E}{\partial y_o^5} \frac{\partial y_o^5}{\partial q} = \eta_q \delta^5 (\underline{\phi} - \overline{\phi}) \\ &= \eta_q \frac{(n+1)\tau}{w_o^{n+2}} |e_{o_1}| (\underline{\phi} - \overline{\phi}) \end{aligned} \tag{31}$$

The update law of the weight a is calculated as

$$\begin{aligned} \frac{\partial y_o^5}{\partial a_{i,j}} &= \frac{\partial y_o^5}{\partial \overline{\phi}} \frac{\partial \overline{\phi}}{\partial a_{i,j}} + \frac{\partial y_o^5}{\partial \underline{\phi}} \frac{\partial \underline{\phi}}{\partial a_{i,j}} \\ &= \frac{\partial y_o^5}{\partial \overline{\phi}} \frac{\partial \overline{\phi}}{\partial f_{i,j}} \frac{\partial f_{i,j}}{\partial a_{i,j}} + \frac{\partial y_o^5}{\partial \underline{\phi}} \frac{\partial \underline{\phi}}{\partial f_{i,j}} \frac{\partial f_{i,j}}{\partial a_{i,j}} \\ &= (1-q)\widetilde{\overline{w}}_{i,j} x_{i,j} + q\widetilde{\underline{w}}_{i,j} x_{i,j} \\ &= ((1-q)\widetilde{\overline{w}}_{i,j} + q\widetilde{\underline{w}}_{i,j}) x_{i,j} \end{aligned} \tag{32}$$

$$\begin{aligned} \Delta a_{i,j} &= -\eta_a \frac{\partial E}{\partial a_{i,j}} = -\eta_a \frac{\partial E}{\partial y_o^5} \frac{\partial y_o^5}{\partial a_{i,j}} = \eta_a \delta^5 \frac{\partial y_o^5}{\partial a_{i,j}} \\ &= \eta_a \frac{(n+1)\tau}{w_o^{n+2}} |e_{o_1}| \Big((1-q)\widetilde{\overline{w}}_{i,j} + q\widetilde{\underline{w}}_{i,j} \Big) x_{i,j} \end{aligned} \tag{33}$$

The update law of the weight b is calculated as

$$\begin{aligned} \frac{\partial y_o^5}{\partial b_{i,j}} &= \frac{\partial y_o^5}{\partial \overline{\phi}} \frac{\partial \overline{\phi}}{\partial b_{i,j}} + \frac{\partial y_o^5}{\partial \underline{\phi}} \frac{\partial \underline{\phi}}{\partial b_{i,j}} \\ &= (1-q)\widetilde{\overline{w}}_{i,j} + q\widetilde{\underline{w}}_{i,j} \end{aligned} \tag{34}$$

$$\begin{aligned} \Delta b_{i,j} &= -\eta_b \frac{\partial E}{\partial b_{i,j}} = -\eta_b \frac{\partial E}{\partial y_o^5} \frac{\partial y_o^5}{\partial b_{i,j}} = \eta_b \delta^5 \frac{\partial y_o^5}{\partial b_{i,j}} \\ &= \eta_b \frac{(n+1)\tau}{w_o^{n+2}} |e_{o_1}| ((1-q)\widetilde{\overline{w}}_{i,j} + q\widetilde{\underline{w}}_{i,j}) \end{aligned} \tag{35}$$

where η_a, η_b, and η_q are the learning rate parameters of the weights a, b, and q, respectively.

Finally, these weights are updated by the following equations.

$$q(N+1) = q(N) + \Delta q \tag{36}$$

$$a_{i,j}(N+1) = a_{i,j}(N) + \Delta a_{i,j} \tag{37}$$

$$b_{i,j}(N+1) = b_{i,j}(N) + \Delta b_{i,j} \tag{38}$$

3.4. Controller Design and Stability Analysis

In this section, an ASMC based on the improved LESO is designed for the n-order uncertain nonlinear system represented by Equation (1).

First, define the systematic error vector as

$$E = X - X_m = \left[e, \dot{e}, \cdots, e^{(n-1)} \right]^T \in R^{n \times 1} \tag{39}$$

The sliding mode variable is designed as

$$s = CE \tag{40}$$

where

$$C = [c_1, c_2, \cdots, c_n] \in R^{1 \times n},$$

C is chosen so that the zeros of the polynomial lie in the left half of the complex plane.

The derivation of the sliding mode variable is defined as

$$\begin{aligned}\dot{s} = C\dot{E} &= [c_1, c_2, \cdots, c_n]\begin{bmatrix}\dot{e}\\ e^{(2)}\\ \vdots\\ e^{(n)}\end{bmatrix}\\ &= c_1\dot{e} + c_2e^{(2)} + \cdots + c_{n-1}e^{(n-1)} + c_n(x^n - x_m^n)\\ &= c_1\dot{e} + c_2e^{(2)} + \cdots + c_{n-1}e^{(n-1)} + c_n(f + b_ou - x_m^n)\end{aligned} \tag{41}$$

Let $\dot{s} = 0$, and it can be deduced that the equivalent control law u_{eq} is defined as

$$u_{eq} = \frac{1}{b_o}(-f + x_m^n) - \frac{1}{c_nb_o}(c_1\dot{e} + c_2e^{(2)} + \cdots + c_{n-1}e^{(n-1)}) \tag{42}$$

The total disturbance f is unknown, so the observation value of LESO is used instead, and the observation error is compensated by adding an adaptive switching term. At this time, the real control rate is obtained as follows

$$u = \frac{1}{b_o}(-z_{n+1} + x_m^n) - \frac{1}{c_nb_o}(c_1\dot{e} + c_2e^{(2)} + \cdots + c_{n-1}e^{(n-1)}) - \widehat{K}sign(s) \tag{43}$$

Theorem 1. *Consider a class of nonlinear uncertain systems with a single input and a single output represented by Equation (1) with partially unknown parameters. Under the premise of satisfying Assumptions 1 and 2, as long as the following conditions are met, the system can be guaranteed to be asymptotically stable.*

(1) The proposed controller is designed as Equation (43).
(2) The parameter adaptation laws of the IT2FNN are designed as Equations (36)–(38).
(3) The adaptive law of ASMC is shown as

$$\dot{\widehat{K}} = \gamma c_nb_o|s| \tag{44}$$

where γ is the learning rate, which is a positive constant.

Proof. The Lyapunov function candidate is designed as

$$V = \frac{1}{2}s^2 + \frac{1}{2\gamma}(\widehat{K} - K^*)^2 \tag{45}$$

Then, define the estimation errors of the adaptive switching term as

$$e_K = \widehat{K} - K^* \tag{46}$$

The derivative of the Lyapunov candidate function is as

$$\begin{aligned}\dot{V} &= s\dot{s} + \tfrac{1}{\gamma}\dot{\widehat{K}}(\widehat{K} - K^*)\\ &= s(c_1\dot{e} + c_2e^{(2)} + \cdots + c_{n-1}e^{(n-1)} + c_n(f + b_ou - x_m^n))) + \tfrac{1}{\gamma}\dot{\widehat{K}}(\widehat{K} - K^*)\\ &= s(c_n(f - z_{n+1}) - b_oc_n\widehat{K}sign(s)) + \tfrac{1}{\gamma}\dot{\widehat{K}}(\widehat{K} - K^*)\\ &= c_ns(e_{o_{n+1}} - b_o\widehat{K}sign(s)) + \tfrac{1}{\gamma}\dot{\widehat{K}}(\widehat{K} - K^*)\\ &= c_nse_{o_{n+1}} - c_nb_o\widehat{K}|s| + \tfrac{1}{\gamma}\dot{\widehat{K}}(\widehat{K} - K^*)\\ &= c_nse_{o_{n+1}} - c_nb_o\widehat{K}|s| + \tfrac{1}{\gamma}(\gamma c_nb_o|s|)(\widehat{K} - K^*)\\ &= c_nse_{o_{n+1}} - c_nb_o|s|K^*\end{aligned} \tag{47}$$

Assuming $e_{o_{n+1}}$ has upper bound as $\left|e_{o_{n+1}}\right| < B_o$, then we can get

$$\begin{aligned} \dot{V} &= c_n s e_{o_{n+1}} - c_n b_o |s| K^* \\ &\leq -c_n |s| (b_o K^* - B_o) \end{aligned} \tag{48}$$

Therefore, the conditions for asymptotic stability of the system are defined as

$$K^* > \frac{1}{b_o} B_o \tag{49}$$

If the condition of Equation (49) is satisfied, then $\dot{V} \leq 0$. Integrating $\dot{V}$ with respect to time, we can find

$$\int_0^t |s| dt \leq \frac{1}{c_n (b_o K^* - B_o)} (V(t) - V(0)).$$

Since $V(0)$ is bounded and $V(t)$ is nonincreasing, it is concluded that $\lim_{t\to\infty} \int_0^t |s| dt$ is bounded. According to Barbalat lemma, one can deduce that

$$\lim_{t\to\infty} s(t) = 0, \ \lim_{t\to\infty} e(t) = 0,$$

which means the tracking error and sliding surface will converge to zero asymptotically. □

4. Algorithm Verification

To verify the practicability and generality of the proposed control strategy, simulations are designed for an inverted pendulum system and an active power filter system. In the simulation, the simulation software used is Matlab/Simulink, and the Matlab software version is 2019b. In addition, the computer system is 64-bit, the CPU is i7-6500U (2.5GHz).

A. Example 1: Single-phase Active power filter

This part takes the single-phase parallel APF as the control object, and it adopts the proposed ASMC-LESO strategy for the first-order dynamic model, obtained by the averaging method, to realize the current control task. The circuit model diagram of APF is given in Figure 3.

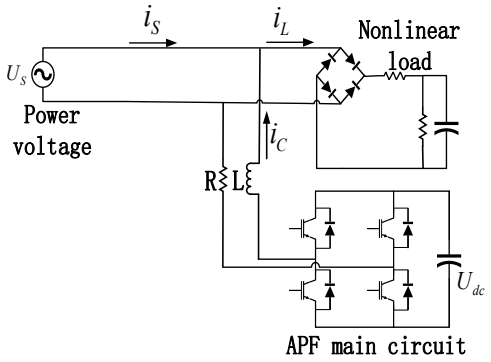

Figure 3. Circuit model diagram of the APF system.

With the development of power electronics technology, a large number of electronic devices, such as air conditioners and microwave ovens, have entered the home. These non-linear loads will produce a large amount of harmonic pollution in the power system, which is very harmful to production and life. The specific performance is that the grid current is distorted, thereby affecting the power quality and causing many safety problems. APF is the most effective harmonic control method, and its working principle can be summarized as: First, the harmonic components added on the load side are calculated by the single-phase harmonic fast detection algorithm, and then, the designed inverter

built with IGBTs is used to generate a compensation current as large as the reverse of the harmonic components to achieve active compensation. Therefore, the control task is to design the controller to output an appropriate duty cycle to control the correct switching of the IGBT, according to the calculated reference current, so as to realize the high-precision tracking control task of the current. In addition, the IGBT switching signal is output by triangular carrier modulation, and the switching frequency of IGBT is 10 khz.

According to the derivation of the circuit model, the first-order model of APF can be obtained as

$$\dot{x} = f(x) + bu + d(t) \tag{50}$$

where

$$x = i_c,\ f(x) = -\frac{R}{L}x - \frac{U_s + U_{dc}}{L},\ b = \frac{2U_{dc}}{L},$$

$d(t)$ is the external disturbance. For the detailed modeling process, please refer to [43].

Therefore, according to the results in Section 3, it can be deduced that the LESO and control law for the APF system is as follows

$$\begin{cases} \dot{z}_1 = z_2 - \beta_1(z_1 - x_1) + b_o u \\ \dot{z}_2 = -\beta_2(z_1 - x_1) \end{cases} \tag{51}$$

$$u = \frac{1}{b_o}(-z_2 + i_r) - \widehat{K}sign(s) \tag{52}$$

where z_1 is the observed value of system state x, z_2 is the extended total disturbance, β_1, β_2 is the observer gain, $b_o = 2U_{dc}/L$, i_r is the reference current, and $s = c_1 e$ where $c_1 = 1$.

In Table 1, the parameters used in the system simulation are given in detail. In the simulation, it is set to connect to the APF main circuit for control at 0 s and add a nonlinear load at 0.6 s. Before the APF is connected, the power supply current contains severe harmonic distortion due to the influence of the nonlinear load on the load side. Figure 4 shows the waveforms of load current i_L, compensation current i_c, and power supply current i_s after the APF is connected. It can be seen from the first load current curve that the current on the load side presents a periodic and severely distorted non-sinusoidal waveform. At the same time, it can be seen from the third power supply current curve that the distortion of the power supply current is gradually controlled to an ideal sinusoidal waveform from the beginning, and the harmonic compensation task is completed in a short time. This is due to the fact that, after the APF is connected, a compensation current that is opposite to the load harmonics is generated. As shown in the second curve in Figure 4, the compensation current enters a steady state process after a short period of adjustment. In more detail, the compensation and reference current tracking comparison curves and error curves are given in Figure 5. It can be said that the compensation current can track the reference current quickly and without overshoot, and the error basically converges after 0.02 s.

Table 1. System parameters in simulation.

Parameter	Value
Grid voltage and frequency	24 V/50 Hz
Non-linear load in steady state	$R1 = 5\ \Omega,\ R2 = 15\ \Omega,\ C = 1e^{-3}$ F
Additional non-linear loads in parallel	$R1 = 15\ \Omega,\ R2 = 15\ \Omega,\ C = 1e^{-3}$ F
Additional R-L loads in parallel	$R = 10\ \Omega,\ L = 200e^{-3}$ H
Main circuit parameter	$L = 18e^{-3}$ H, $R = 1\Omega,\ V_{ref} = 50$ V
Sampling time	$T_s = 1e^{-5}$ s

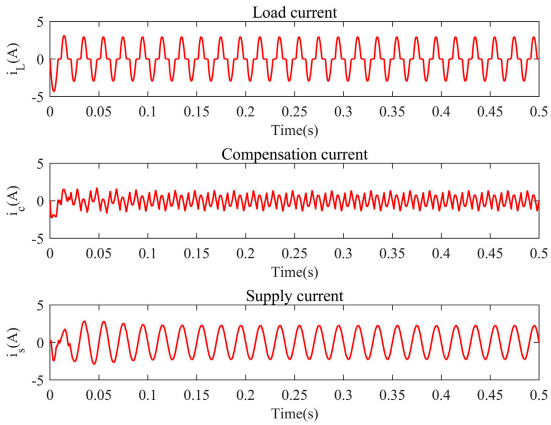

Figure 4. Current curves of steady-state response.

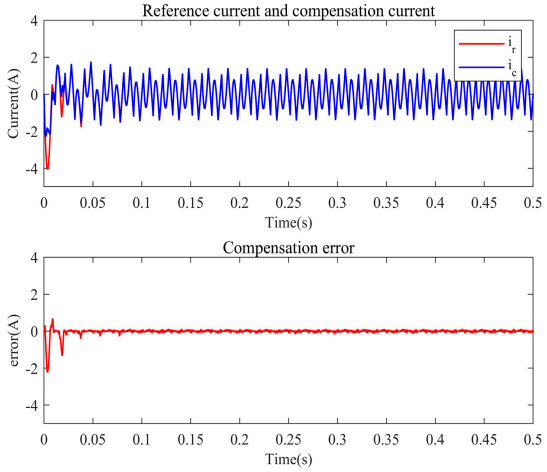

Figure 5. Current tracking comparison and tracking error curves.

To accurately compare the performance of APF, Figures 6 and 7 show the power supply current spectrum when the APF is just connected (0 s) and when it enters the steady state (0.2 s), respectively. It can be seen that, when the controller is just connected at 0 s, the power supply current has a large number of low-order and some high-order harmonic content, and the total harmonic distortion rate (THD) reaches 26.95%, which is far from meeting the requirements of international standards of less than 5%. However, after adopting the proposed control method, the system entered a steady state at 0.2 s, and it can be seen from Figures 6 and 7 that the harmonic components are greatly reduced, and the THD is only 2.10%, which means that a good harmonic suppression task is achieved.

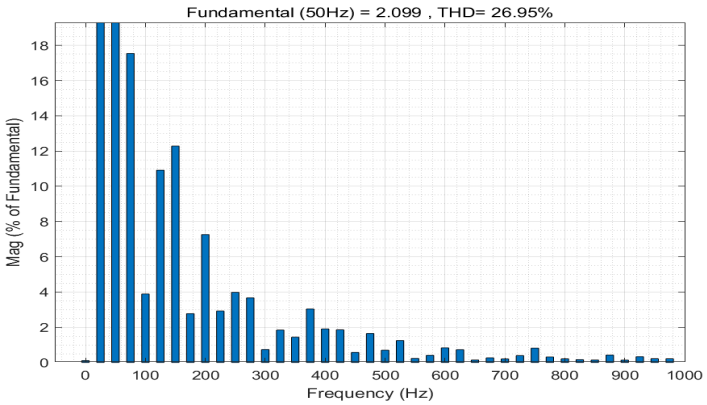

Figure 6. Spectrogram of supply current after access to APF at 0 s.

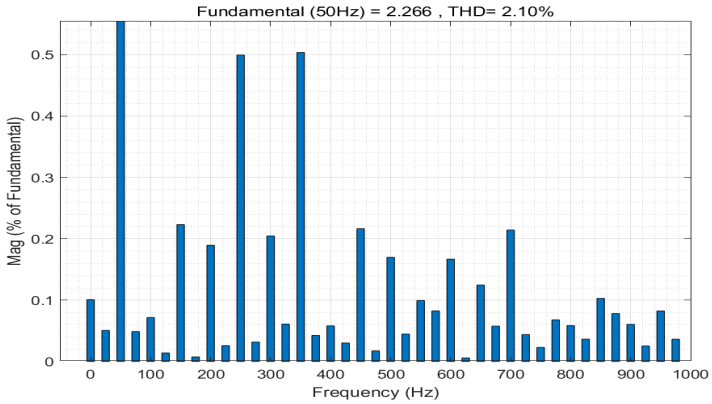

Figure 7. Spectrogram of supply current in steady state at 0.2 s.

In addition, the estimated curve of IT2FNN for observer bandwidth w_o is given in Figure 8, showing after a short adaptive learning and correction, the output of the neural network converges to about 3800, realizing real-time estimation of the observer bandwidth. On this basis, the state estimation curve of LESO is given in Figure 9, where it is shown that LESO also achieves accurate tracking of the system state after the bandwidth has converged, and the red and blue curves almost completely coincide. At the same time, the estimated curve of the total disturbance is shown in the lower half of Figure 9, showing a periodic sine wave-like curve with an amplitude ranging from -6000 to 0, which is basically consistent with the nominal model. In general, the total disturbance estimates are also relatively accurate. Then, the adaptive curve of the switching term gain is shown in Figure 10. The gain of the switching term converges to about 0.24 in a very short time, and the gain value is small, which will not cause serious chattering, and indirectly shows that the LESO has a good estimation effect on the total disturbance.

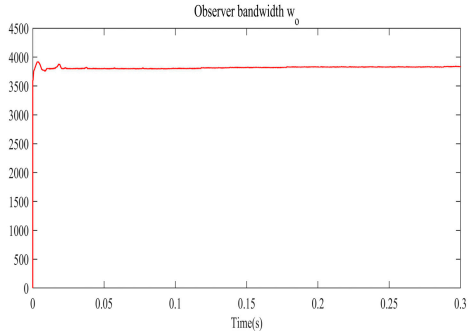

Figure 8. Learning curve of IT2FNN for observer bandwidth w_o in APF.

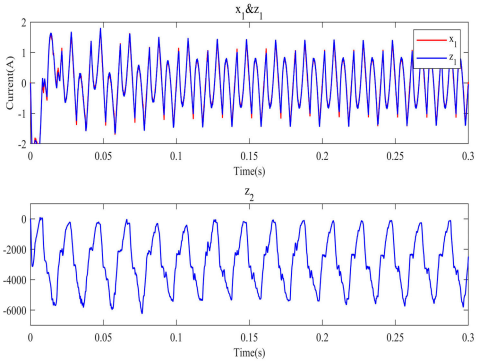

Figure 9. Observation curves of LESO for system state and total disturbance in APF.

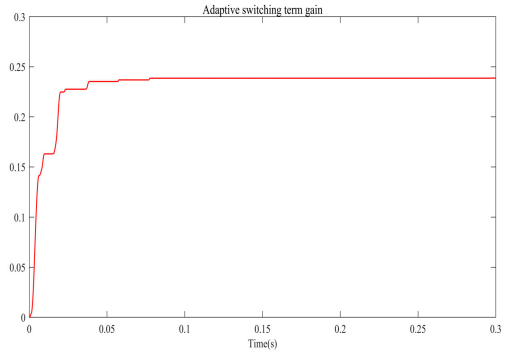

Figure 10. Adaptive curve of switching term gain of ASMC in APF.

Remark 3. *The total disturbance $f_{td}(x)$ includes the system dynamics, $(b - \widehat{b})u$ and the external disturbance $d(t)$. It can be seen from Equation (50) that the APF system dynamics $f(x)$ is theoretically an ideal sinusoid. However, since the value of the resistance and inductance is affected by the environment and the power supply voltage and DC side voltage will also fluctuate, then considering $(b - \widehat{b})u$ and external disturbances, the estimated total disturbance will fluctuate larger than the $f(x)$ of the nominal model. The total disturbance curve estimated by the system is shown in Figure 9, which shows that the total disturbance is indeed an irregular nonlinear function.*

Finally, to show the superiority of the proposed controller, the comparison results and analysis with the ASMC method are presented. Figure 11 shows the current tracking comparison curve and the error comparison curve for the two methods. As can be seen, under the comparative ASMC method, there is obvious overshoot and runaway state in the early control stage because it does not have LESO to accurately observe and compensate the total disturbance of the uncertain system. In addition, even in steady state, although the adaptive gain keeps increasing to offset the uncertainty, there is always a periodic large steady state error. The above phenomenon shows that the high-gain switching term, solely relying on the adaptive sliding mode control, cannot completely offset the uncertainty caused by the unknown dynamics, and there are always some disturbances that cannot be compensated. This shows that the proposed ASMC-LESO method is more robust and practical than AMSC. In addition, in theory, since the LESO prior actively compensates for the unknown uncertainty disturbance, the adaptive gain will be relatively small, thereby weakening the chattering verified in Figure 12, showing the comparison curves of the output chattering under the two methods. It can be clearly seen that the variation amplitude and variation frequency of the control output of the proposed method are smaller, which means that the chattering is smaller. More specifically, the variances of the control outputs under the AMSC-LESO and ASMC methods are calculated to be 0.1539 and 1.6618, respectively, which are significantly different by an order of magnitude.

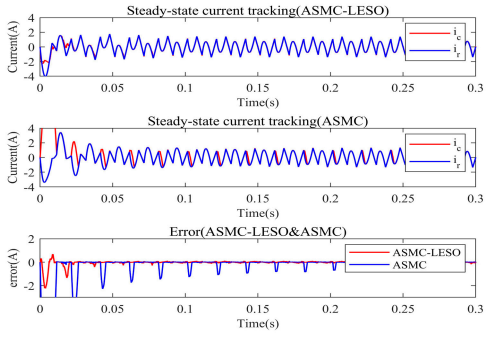

Figure 11. Tracking and error comparison curves of the ASMC-LESO and ASMC.

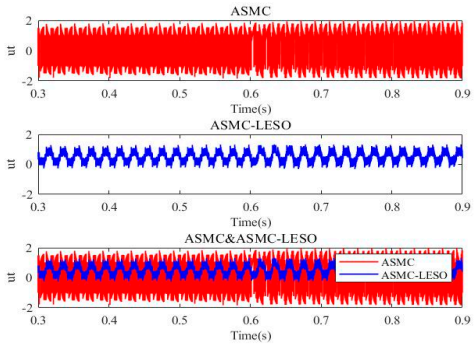

Figure 12. Comparison curve of output chattering of the ASMC-LESO and ASMC.

Further, THD comparison between ASMC-LESO and ASMC is shown in Table 2. In the initial control, the THD under the ASMC-LESO and ASMC methods are 26.95% and 67.01%, respectively, and the performance is very different, which is because the ASMC method has the disadvantages of slow response, overshoot, and runaway in the initial control. Then, the THD of the ASMC-LESO under steady state is 2.10%, which is 1.23% lower than 3.33% of the ASMC. A nonlinear load is added on the user side at 0.6 s, so the THD of the two methods also abruptly increased to 8.43% and 9.10%, respectively, when the load suddenly increased. Then, after a short control adjustment, it entered a new steady state, at which time the THD of the two methods were 1.26% and 2.91%, respectively. Overall, regardless of the state, the proposed ASMC-LESO method always has a smaller THD and better harmonic compensation capability than the comparison methods.

Table 2. THD performance comparison of different methods.

State\Strategy	THD of ASMC-LESO	THD of ASMC
Initial period	26.95%	67.01%
Steady state	2.10%	3.33%
When load increase	8.43%	9.10%
After load increase	1.26%	2.91%

B. Example 2: Single-stage Inverted Pendulum System

The second-order dynamic model of the single-stage inverted pendulum is as

$$\begin{cases} \dot{x}_1 = x_2 \\ \dot{x}_2 = f(x) + bu \\ y = x_1 \end{cases} \tag{53}$$

where

$$f(x) = \frac{g \sin x_1 - mlx_2^2 \cos x_1 \sin x_1/(m_c+m)}{l[4/3 - m\cos^2 x_1/(m_c+m)]},\ b = \frac{\cos x_1/(m_c+m)}{l[4/3 - m\cos^2 x_1/(m_c+m)]},\ g = 9.8\ \mathrm{m/s^2}$$

g is the acceleration of gravity, $m_c = 1$ kg is the mass of the car, $m = 0.1$ kg is the mass of the pendulum, $l = 0.5$ m is half of the pendulum length, x_1 and x_2 are the swing angle and swing speed, the initial state of the system is $[\pi/60\ 0]$, and the expected trajectory is $y_d = 0.1 \sin t$.

Therefore, according to the results in Section 3, it can be deduced that the LESO and control law for the inverted pendulum system are as follows

$$\begin{cases} \dot{z}_1 = z_2 - \beta_1(z_1 - x_1) \\ \dot{z}_2 = z_3 - \beta_2(z_1 - x_1) + b_o u \\ \dot{z}_3 = -\beta_3(z_1 - x_1) \end{cases} \tag{54}$$

$$u = \frac{1}{b_o}(-z_3 + \ddot{y}_d) - \frac{1}{c_2 b_o}(c_1 \dot{e}) - \widehat{K} sign(s) \tag{55}$$

where

$$b_o = 1.46,\ C = [c_1\ c_2] = [100\ 1],\ s = 100e + \dot{e},$$

y_d is the reference current.

The angle tracking curve and tracking error curve are given in Figure 13. Within 1 s, the swing angle of the inverted pendulum completely and accurately tracks the reference angle, and the error also converges to 0. Moreover, Figure 14 shows the observe bandwidth curve in the output of the IT2FNN, which converges to 99.9 within 1 s.

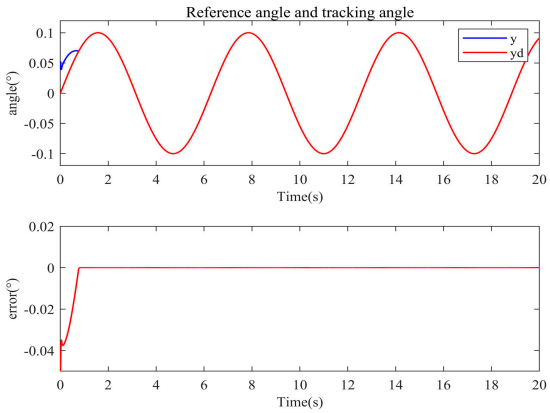

Figure 13. Angle tracking curve and error curve.

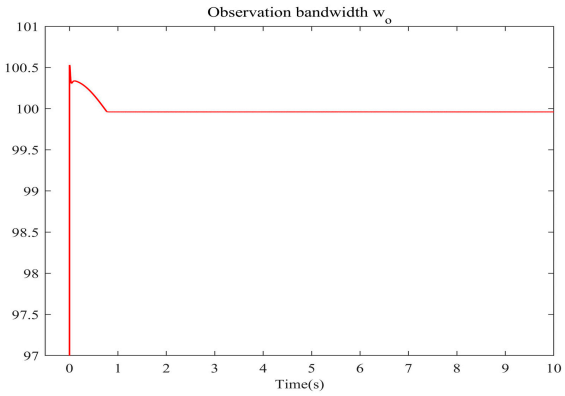

Figure 14. Learning curve of IT2FNN for observer bandwidth w_o in the inverted pendulum system.

The observation and comparison curves of LESO for system states x_1, x_2, and total disturbance f are shown in Figure 15. The red curve in the figure is the system state, and the blue curve is the observation curve. It can be seen that the two almost completely overlap after 0.1 s, which means that the observation effect of LESO is very good, and the system state can be accurately estimated. Further, Figure 16 shows the observation error curves of the three states. It can be seen, more intuitively, that the observation errors of the three states are very small, and the observation error magnitudes of x_1, x_2, and x_3 reach $1e-6$, $1e-4$, and $1e-2$, respectively. Finally, the adaptive curve for the gain of the switching term is given in Figure 17, which also converges to around 5.5 within 1 s.

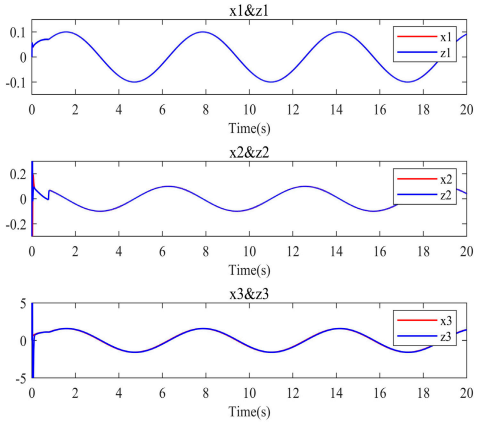

Figure 15. Observation curves of LESO for system state and total disturbance in the inverted pendulum system.

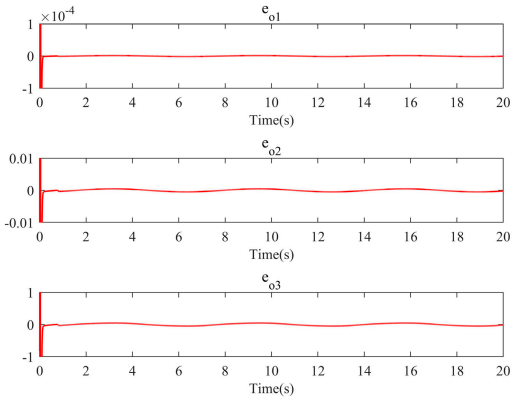

Figure 16. Observe error curves of LESO for system state and total disturbance in the inverted pendulum system.

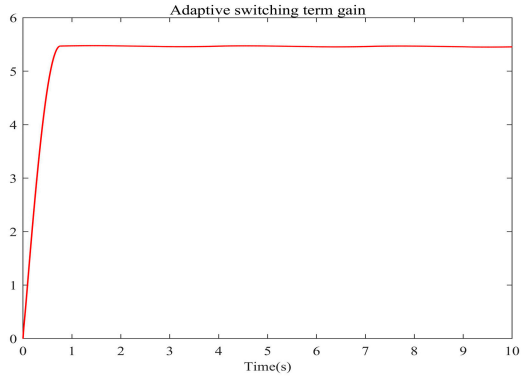

Figure 17. Adaptive curve of switching term gain of ASMC in the inverted pendulum system.

5. Conclusions

A LESO-based adaptive sliding mode control using IT2FNN is established for uncertain nonlinear systems. The proposed general control strategy solves the bandwidth parameter optimization problem of LESO, using IT2FNN to realize the real-time estimation of the observation bandwidth, so as to ensure that LESO can effectively and accurately estimate the total disturbance of the system and realize active compensation. Then, the stability of the system is guaranteed by adaptive sliding mode control, which is designed by the Lyapunov stability theory. Finally, the simulations verified that the proposed control strategy has good practicability and versatility.

Author Contributions: Conceptualization, L.L. and J.F.; software and validation, L.L. and X.Y.; writing—original draft preparation, L.L.; writing—review and editing, J.F. All authors have read and agreed to the published version of the manuscript.

Funding: This work is support by the University Graduate Research and Innovation Projects of Jiangsu Province under Grant No. KYCX22_0608, National Science Foundation of China (Grant No. 62273131, 61873085), and the Fundamental Research Funds for the Central Universities under Grant No. 4200261671.

Data Availability Statement: Not applicable.

Conflicts of Interest: The authors declare no conflict of interest.

References

1. Ginoya, D.; Shendge, P.D.; Phadke, S.B. Sliding Mode Control for Mismatched Uncertain Systems Using an Extended Disturbance Observer. *IEEE Trans. Ind. Electron.* **2014**, *61*, 1983–1992. [CrossRef]
2. Ang, K.; Chong, G.; Li, Y. PID Control System Analysis, Design, and Technology. *IEEE Trans. Control. Syst. Technol.* **2005**, *13*, 559–576.
3. Narendra, K.; Balakrishnan, J. Adaptive control using multiple models. *IEEE Trans. Autom. Control* **1997**, *42*, 171–187. [CrossRef]
4. Hong, Y.; Wang, J.; Cheng, D. Adaptive Finite-Time Control of Nonlinear Systems with Parametric Uncertainty. *IEEE Trans. Autom. Control* **2006**, *51*, 858–862. [CrossRef]
5. Li, J.; Zhou, S.; Xu, S. Fuzzy Control System Design via Fuzzy Lyapunov Functions. *IEEE Trans. Syst. Man Cybern. Part B (Cybern.)* **2008**, *38*, 1657–1661. [CrossRef]
6. Wang, A.; Liu, L.; Qiu, J.; Feng, G. Event-Triggered Robust Adaptive Fuzzy Control for a Class of Nonlinear Systems. *IEEE Trans. Fuzzy Syst.* **2019**, *27*, 1648–1658. [CrossRef]
7. Xu, B. Composite Learning Control of Flexible-Link Manipulator Using NN and DOB. *IEEE Trans. Syst. Man Cybern. Syst.* **2018**, *48*, 1979–1985. [CrossRef]
8. Liaw, H.C.; Shirinzadeh, B.; Smith, J. Sliding-Mode Enhanced Adaptive Motion Tracking Control of Piezoelectric Actuation Systems for Micro/Nano Manipulation. *IEEE Trans. Control. Syst. Technol.* **2008**, *16*, 826–833. [CrossRef]
9. Wu, W.; Liu, T. Frequency-shaped sliding mode control for flying height of pickup head in near-field optical disk drives. *IEEE Trans. Magn.* **2005**, *41*, 1061–1063. [CrossRef]
10. Silva, J. Sliding-mode control of boost-type unity-power-factor PWM rectifiers. *IEEE Trans. Ind. Electron.* **1999**, *46*, 594–603. [CrossRef]
11. Yu, H.-C.; Liu, T.S. Output Feedback Sliding Mode Control for a Linear Focusing Actuator in Digital Video Cameras. *IEEE Trans. Magn.* **2007**, *43*, 4048–4050. [CrossRef]
12. Xu, Q. Piezoelectric Nanopositioning Control Using Second-Order Discrete-Time Terminal Sliding-Mode Strategy. *IEEE Trans. Ind. Electron.* **2015**, *62*, 7738–7748. [CrossRef]
13. Yao, X.; Park, J.H.; Dong, H.; Guo, L.; Lin, X. Robust Adaptive Nonsingular Terminal Sliding Mode Control for Automatic Train Operation. *IEEE Trans. Syst. Man Cybern. Syst.* **2019**, *49*, 2406–2415. [CrossRef]
14. Wang, W.; Ma, J.; Li, X.; Cheng, Z.; Zhu, H.; Teo, C.S.; Lee, T.H. Iterative Super-Twisting Sliding Mode Control for Tray Indexing System with Unknown Dynamics. *IEEE Trans. Ind. Electron.* **2021**, *68*, 9855–9865. [CrossRef]
15. Fei, J.; Feng, Z. Fractional-Order Finite-Time Super-Twisting Sliding Mode Control of Micro Gyroscope Based on Double-Loop Fuzzy Neural Network. *IEEE Trans. Syst. Man Cybern. Syst.* **2021**, *51*, 7692–7706. [CrossRef]
16. Chang, Y. Adaptive Sliding Mode Control of Multi-Input Nonlinear Systems with Perturbations to Achieve Asymptotical Stability. *IEEE Trans. Autom. Control* **2009**, *54*, 2863–2869. [CrossRef]
17. Yoo, B.; Ham, W. Adaptive fuzzy sliding mode control of nonlinear system. *IEEE Trans. Fuzzy Syst.* **1998**, *6*, 315–321. [CrossRef]
18. Oucheriah, S.; Guo, L. PWM-Based Adaptive Sliding-Mode Control for Boost DC–DC Converters. *IEEE Trans. Ind. Electron.* **2013**, *60*, 3291–3294. [CrossRef]
19. Hornik, K.; Stinchcombe, M.; White, H. Multilayer feedforward networks are universal approximators. *Neural Netw.* **1989**, *2*, 359–366. [CrossRef]
20. Chen, Z.; Huang, F.; Chen, W.; Zhang, J.; Sun, W.; Chen, J.; Gu, J.; Zhu, S. RBFNN-Based Adaptive Sliding Mode Control Design for Delayed Nonlinear Multilateral Telerobotic System with Cooperative Manipulation. *IEEE Trans. Ind. Inform.* **2020**, *16*, 1236–1247. [CrossRef]
21. Fei, J.; Chen, Y.; Liu, L.; Fang, Y. Fuzzy Multiple Hidden Layer Recurrent Neural Control of Nonlinear System Using Terminal Sliding-Mode Controller. *IEEE Trans. Cybern.* **2021**, *52*, 9519–9534. [CrossRef] [PubMed]
22. Fei, J.; Wang, H.; Fang, Y. Novel Neural Network Fractional-Order Sliding-Mode Control with Application to Active Power Filter. *IEEE Trans. Syst. Man Cybern. Syst.* **2022**, *52*, 3508–3518. [CrossRef]
23. Han, J. From PID to Active Disturbance Rejection Control. *IEEE Trans. Ind. Electron.* **2009**, *56*, 900–906. [CrossRef]
24. Lin, F.-J.; Wai, R.-J.; Hong, C.-M. Recurrent neural network control for LCC-resonant ultrasonic motor drive. *IEEE Trans. Ultrason. Ferroelectr. Freq. Control.* **2000**, *47*, 737–749. [CrossRef] [PubMed]

25. Chu, Y.; Fei, J.; Hou, S. Adaptive Global Sliding-Mode Control for Dynamic Systems Using Double Hidden Layer Recurrent Neural Network Structure. *IEEE Trans. Neural Netw. Learn. Syst.* **2020**, *31*, 1297–1309. [CrossRef] [PubMed]
26. Fei, J.; Chen, Y. Fuzzy Double Hidden Layer Recurrent Neural Terminal Sliding Mode Control of Single-Phase Active Power Filter. *IEEE Trans. Fuzzy Syst.* **2021**, *29*, 3067–3081. [CrossRef]
27. Liu, Y.-C.; Laghrouche, S.; N'Diaye, A.; Cirrincione, M. Hermite neural network-based second-order sliding-mode control of synchronous reluctance motor drive systems. *J. Frankl. Inst.* **2021**, *358*, 400–427. [CrossRef]
28. Fei, J.; Wang, Z.; Pan, Q. Self-Constructing Fuzzy Neural Fractional-Order Sliding Mode Control of Active Power Filter. *IEEE Trans. Neural Netw. Learn. Syst.* **2022**, 1–12. [CrossRef]
29. Fei, J.; Wang, Z.; Fang, Y. Self-Evolving Chebyshev Fuzzy Neural Fractional-Order Sliding Mode Control for Active Power Filter. *IEEE Trans. Ind. Inform.* **2022**, 1. [CrossRef]
30. Luenberger, D. An Introduction to Observers. *IEEE Trans. Autom. Control* **1971**, *16*, 596–602. [CrossRef]
31. Jo, N.H.; Jeon, C.; Shim, H. Noise Reduction Disturbance Observer for Disturbance Attenuation and Noise Suppression. *IEEE Trans. Ind. Electron.* **2017**, *64*, 1381–1391. [CrossRef]
32. Ran, M.; Wang, Q.; Dong, C. Active Disturbance Rejection Control for Uncertain Nonaffine-in-Control Nonlinear Systems. *IEEE Trans. Autom. Control* **2017**, *62*, 5830–5836. [CrossRef]
33. Wang, H.; Shi, L.; Man, Z.; Zheng, J.; Li, S.; Yu, M.; Jiang, C.; Kong, H.; Cao, Z. Continuous Fast Nonsingular Terminal Sliding Mode Control of Automotive Electronic Throttle Systems Using Finite-Time Exact Observer. *IEEE Trans. Ind. Electron.* **2018**, *65*, 7160–7172. [CrossRef]
34. Won, D.; Kim, W.; Tomizuka, M. Nonlinear Control with High-Gain Extended State Observer for Position Tracking of Electro-Hydraulic Systems. *IEEE/ASME Trans. Mechatron.* **2020**, *25*, 2610–2621. [CrossRef]
35. Sun, B.; Gao, Z. A DSP-Based Active Disturbance Rejection Control Design for a 1-kW H-Bridge DC–DC Power Converter. *IEEE Trans. Ind. Electron.* **2005**, *52*, 1271–1277. [CrossRef]
36. Zhao, L.; Yang, Y.; Xia, Y.; Liu, Z. Active Disturbance Rejection Position Control for a Magnetic Rodless Pneumatic Cylinder. *IEEE Trans. Ind. Electron.* **2015**, *62*, 5838–5846. [CrossRef]
37. Zhao, Z.-L.; Guo, B.-Z. A nonlinear extended state observer based on fractional power functions. *Automatica* **2017**, *81*, 286–296. [CrossRef]
38. Gao, Z. Scaling and bandwidth-parameterization based controller tuning. In Proceedings of the 2003 American Control Conference, Denver, CO, USA, 4–6 June 2003; pp. 4989–4996. [CrossRef]
39. Xue, W.; Bai, W.; Yang, S.; Song, K.; Huang, Y.; Xie, H. ADRC with Adaptive Extended State Observer and its Application to Air–Fuel Ratio Control in Gasoline Engines. *IEEE Trans. Ind. Electron.* **2015**, *62*, 5847–5857. [CrossRef]
40. Wang, S.; Ren, X.; Na, J.; Zeng, T. Extended-State-Observer-Based Funnel Control for Nonlinear Servomechanisms with Prescribed Tracking Performance. *IEEE Trans. Autom. Sci. Eng.* **2017**, *14*, 98–108. [CrossRef]
41. Tan, W.; Fu, C. Linear Active Disturbance Rejection Control: Analysis and Tuning via IMC. *IEEE Trans. Ind. Electron.* **2016**, *63*, 2350–2359. [CrossRef]
42. Zheng, Q.; Gaol, L.Q.; Gao, Z. On stability analysis of active disturbance rejection control for nonlinear time-varying plants with unknown dynamics. In Proceedings of the 2007 46th IEEE Conference on Decision and Control, New Orleans, LA, USA, 12–14 December 2007; pp. 3501–3506. [CrossRef]
43. Liu, L.; Fei, J. Extended State Observer Based Interval Type-2 Fuzzy Neural Network Sliding Mode Control with Its Application in Active Power Filter. *IEEE Trans. Power Electron.* **2022**, *37*, 5138–5154. [CrossRef]